AD-A165 791 HIGH-FREQUENCY CHANNEL DESCRIPTION(U) SRI INTERNATIONAL 1/1
MENLO PARK CA G H PRICE 01 OCT 83 DNA-TR-82-196
DNA001-82-C-0218

UNCLASSIFIED F/G 17/2.1 NL

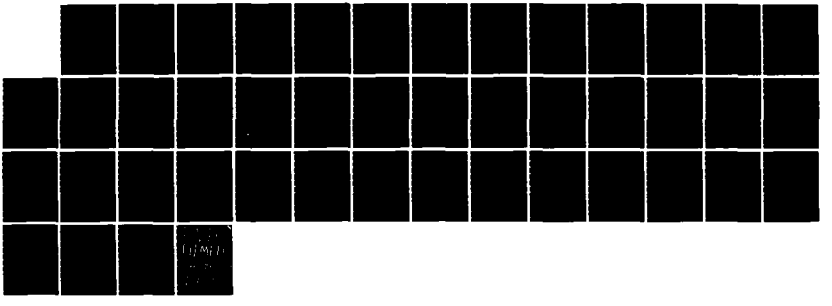

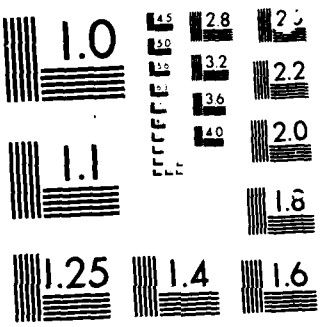

MICROCOPY RESOLUTION TEST CHART

E301931

(12)

AD-A165 791

DNA-TR-82-196

HIGH-FREQUENCY CHANNEL DESCRIPTION

Gary H. Price
SRI International
333 Ravenswood Avenue
Menlo Park, CA 94025-3434

1 October 1983

Technical Report

CONTRACT No. DNA 001-82-C-0218

Approved for public release;
distribution is unlimited.

THIS WORK WAS SPONSORED BY THE DEFENSE NUCLEAR AGENCY
UNDER RDT&E RMSS CODE B322082466 S99QAXHB00015 H2590D.

Prepared for
Director
DEFENSE NUCLEAR AGENCY
Washington, DC 20305-1000

Destroy this report when it is no longer needed. Do not return to sender.

PLEASE NOTIFY THE DEFENSE NUCLEAR AGENCY, ATTN: STTI, WASHINGTON, DC 20305-1000, IF YOUR ADDRESS IS INCORRECT, IF YOU WISH IT DELETED FROM THE DISTRIBUTION LIST, OR IF THE ADDRESSEE IS NO LONGER EMPLOYED BY YOUR ORGANIZATION.

UNCLASSIFIED

SECURITY CLASSIFICATION OF THIS PAGE AD-A165791

REPORT DOCUMENTATION PAGE

Form Approved
OMB No. 0704-0188
Exp. Date: Jun 30, 1986

1a. REPORT SECURITY CLASSIFICATION UNCLASSIFIED	1b. RESTRICTIVE MARKINGS
2a. SECURITY CLASSIFICATION AUTHORITY	3. DISTRIBUTION/AVAILABILITY OF REPORT Approved for public release; distribution is unlimited.
2b. DECLASSIFICATION/DOWNGRADING SCHEDULE N/A since UNCLASSIFIED	
4. PERFORMING ORGANIZATION REPORT NUMBER(S) SRI Project 4571	5. MONITORING ORGANIZATION REPORT NUMBER(S) DNA-TR-82-196
6a. NAME OF PERFORMING ORGANIZATION SRI International 6b. OFFICE SYMBOL (If applicable)	7a. NAME OF MONITORING ORGANIZATION Director Defense Nuclear Agency
6c. ADDRESS (City, State, and ZIP Code) 333 Ravenswood Avenue Menlo Park, California 94025-3434	7b. ADDRESS (City, State, and ZIP Code) Washington, DC 20305-1000
8a. NAME OF FUNDING/SPONSORING ORGANIZATION 8b. OFFICE SYMBOL (If applicable)	9. PROCUREMENT INSTRUMENT IDENTIFICATION NUMBER DNA 001-82-C-0218
8c. ADDRESS (City, State, and ZIP Code)	10. SOURCE OF FUNDING NUMBERS PROGRAM ELEMENT NO. 62715H; PROJECT NO. S99QAXH; TASK NO. B; WORK UNIT ACCESSION NO. DH006204

11. TITLE (Include Security Classification)
HIGH-FREQUENCY CHANNEL DESCRIPTION

12. PERSONAL AUTHOR(S)
Price, Gary H.

13a. TYPE OF REPORT	13b. TIME COVERED	14. DATE OF REPORT (Year, Month, Day)	15. PAGE COUNT
Technical Report	FROM 820611 TO 830511	831001	44

16. SUPPLEMENTARY NOTATION
This work was sponsored by the Defense Nuclear Agency under RDT&E RMSS Code B322082466 S99QAXHB00015 H2590D.

17. COSATI CODES		
FIELD	GROUP	SUB-GROUP
17	2	.1
20	14	

18. SUBJECT TERMS (Continue on reverse if necessary and identify by block number)
Ionospheric Propagation; HF Propagation; HF Sky-Wave Propagation; HF Scatter Model; Scatter Propagation Model; Forward Scatter

19. ABSTRACT (Continue on reverse if necessary and identify by block number)

A recently developed model for the effects of scatter caused by irregularities in the propagation medium on signals propagated via substantially refracted ray paths is evaluated in the context of HF sky wave radio propagation. Previously neglected characteristics of refracted ray paths associated with caustic formation are analyzed, and their effect on the scatter behavior is found to be small.

The conditions necessary for a single, thin phase screen to provide a good description of the scatter effects (the apex approximation) are shown not to be well satisfied under some circumstances for HF sky-waves.

20. DISTRIBUTION/AVAILABILITY OF ABSTRACT ☐ UNCLASSIFIED/UNLIMITED ☒ SAME AS RPT. ☐ DTIC USERS	21. ABSTRACT SECURITY CLASSIFICATION UNCLASSIFIED
22a. NAME OF RESPONSIBLE INDIVIDUAL Betty L. Fox	22b. TELEPHONE (Include Area Code) 202 325-7042; 22c. OFFICE SYMBOL DNA/STTI

DD FORM 1473, 84 MAR 83 APR edition may be used until exhausted. All other editions are obsolete.

SECURITY CLASSIFICATION OF THIS PAGE
UNCLASSIFIED

18. SUBJECT TERMS (Continued)

High-Frequency Radio-Wave Propagation
HF Channel Model

TABLE OF CONTENTS

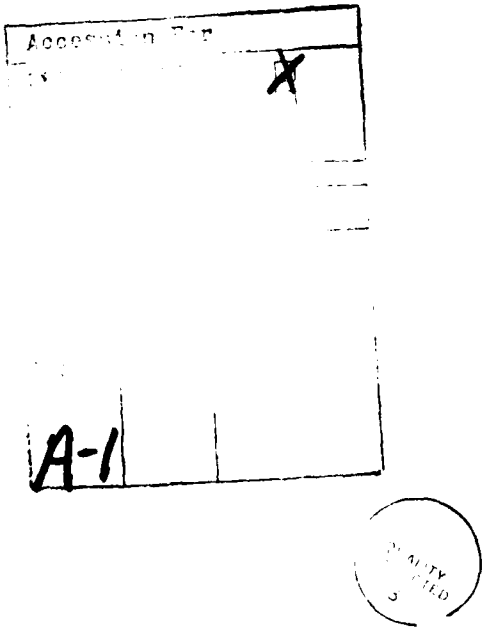

LIST OF ILLUSTRATIONS

SECTION 1
INTRODUCTION

High-frequency (HF) radio signals propagated to large distances by ionospheric refraction remain of practical interest as a means for communication and remote probing (e.g., over-the-horizon radar). Scatter from ionospheric irregularities can strongly affect such signals. An understanding of the effects of such scatter therefore is necessary if the performance of systems that make use of such signals is to be determined.

A useful characterization of scatter effects at HF is available for the natural environment, but it has been attained almost entirely empirically. Our knowledge of the propagation environment following high-altitude nuclear detonations is more fragmentary. High-frequency ionosonde data taken during past nuclear tests confirm the existence of substantial ionospheric irregularity following high-altitude detonations.[1*] These irregularities can be expected to reduce system performance through loss of signal coherence across both frequency and time. The data do not, however, suffice in themselves to provide a complete characterization of scatter effects at HF in the nuclear environment. Thus, a need exists for analytical models, based on a general understanding of such effects, that can be used to predict these effects. This final report describes the work performed to this end under Tasks 1 and 2 of Contract DNA001-82-C-0218. Development of a plan for a field experiment to complement this effort, as called for by Tasks 3 and 4 of this contract, is described in a separate report.[2]

Substantial progress has been achieved in recent years in describing the effects of ionospheric irregularities on higher frequency signals,

---

*Superscripts denote references listed at the end of the report.

such as those used in transionospheric ground-to-satellite communications links and by missile-tracking radar systems. As a result of this progress, the characteristics of the irregularities themselves and of their effects on these higher frequency signals are now much better understood for both natural and nuclear environments. The calculation of irregularity effects is, however, inherently simpler at the higher frequencies than it is at HF. (Compare, for example, the analysis in References 3 and 4.) Consequently, the modeling of scatter effects at HF has received only sporadic attention in the absence of new insights on methods for their calculation.

Current HF nuclear-effects propagation codes, such as NUCOM, describe well the gross multipath effects associated with ionospheric refraction at HF, but they do not address the effects of scatter from ionospheric irregularities. Such scatter can spread the signal substantially both in time and frequency. Our approach to providing a complete time-delay and Doppler spread channel characterization at HF is to deal separately with the scatter effects on each of the possibly several ray paths that constitute the gross multipath. Apart from the strong bending of the HF paths by refraction, each of these paths then resembles a line-of-sight path such as is encountered in transionospheric propagation at higher frequencies.

Recent work by Flatté et al.[5] on the scatter of oceanic acoustic waves has shown this approach to the determination of scatter effects in the presence of strong refraction to be very fruitful. Furthermore, as has been pointed out in recent JASON studies[6], the problem addressed by Flatté et al. is very similar to that of the scatter of obliquely propagating HF radio waves by ionospheric irregularities. The ocean and the ionosphere are sufficiently similar media, in the context of the refractive-index variations they present to signals propagating obliquely through them, for many of the approximations used in the acoustic analysis to remain valid in the ionospheric context. Consequently, adaption of this work to HF radio is relatively straightforward and yields many useful results without inordinate effort.

The results of the analysis undertaken by Flatté et al.[5] also bear, as they emphasize, a clear relationship to the scatter models that have been developed for line-of-sight propagation through slowly-varying media.

The scatter model developed recently by DNA[7] for transionospheric radio-wave propagation is an example of these models. Adaption of the oceanic-scatter theory to HF thus additionally offers the prospect of a unified approach to the calculation of scatter effects in the nuclear environment for both HF and higher frequencies.

A preliminary examination of the scatter theory developed by Flatté et al.[5], although encouraging regarding the above expectations, left us uncertain on certain points as to the approximations involved in its development. The largely hueristic approach adopted by Flatté et al. in their exposition of the theory relies heavily on the use of ray concepts to extend results obtained in the simpler case of propagation through statistically uniform media. These ray concepts, although useful as an expository tool, become suspect in the very regions--namely, near the turning points of rays refracted by the large-scale nonrandom variations in the background medium--that most strongly differentiate the problem from that of a uniform medium. Consequently, we felt it necessary in this initial work to dwell at some length on the precise manner in which these regions contribute to the scatter effects.

This question is examined in Section 3, after a brief introduction to the theory developed by Flatté et al.[5], as adapted by us to HF, in Section 2. In our examination we employ a simple ionospheric model that lends itself to analytic treatment. Difficulties associated with caustics formed by the unscattered ray paths are analyzed, and an improved treatment of the effects of these caustics is described. The practical impact of these effects is found from this examination to be slight.

A further simplification of the theory, the apex approximation, is discussed in Section 4. This approximation attempts to exploit the tendency of scatter to occur most strongly near the apex of a ray path. The example examined by us leads us to conclude that this approximation must be used cautiously at HF.

We finally consider briefly, in Section 5, the r ionship of the theory to the channel parameters that will be measured experimentally. Expressions are given, based on the oce n-scatter results of Flatté et al.[5].

for calculation of the basic parameters that an experiment would be expected to measure. These results are presented in terms of the two theoretical quantities, the scatter strength and diffraction parameters, that characterize the scatter effects. Although the results presented here suffice to demonstrate the completeness and relevance of the theory, further work to develop expressions tailored to HF would be useful.

Section 6 summarizes our results and suggests an approach toward implementation of the theory for HF application.

SECTION 2
PATH-INTEGRAL THEORY

In recent work on the scatter of acoustic signals by oceanic irregularities, Flatté et al.[5] have, under the assumption that small-angle scattering is dominant, expressed the effects of scatter from fluctuations in the refractive index of the propagation medium in terms of an integral over all possible infinitesimally segmented ray paths connecting the transmitter and the receiver. They then demonstrate that the consequent "path-integral" expressions for the received-signal characteristics can be reduced to approximate expressions involving integrals of various quantities taken over the mean (essentially, unscattered) ray path that results from the large-scale (and deterministic) spatial variations in refractive index. In this form, the expressions that describe the scattered field bear a close relationship to those that result in the simpler problem of scatter from fluctuations in an otherwise homogeneous propagation medium. Extension of these results to the more complex case of initially refracted unperturbed ray paths entails, as will be seen below, little more than appropriate generalization of the definitions of key scatter parameters. Further simplifications that can be made in certain cases, such as the thin-phase-screen approximation, also have easily recognized analogs in the theory developed by Flatté and his colleagues.

As is discussed in detail by Flatté et al.,[5] the characteristics of the received signal are determined essentially by the strength and the size of the random inhomogeneities in the propagation medium. These properties of the medium are, in turn, described by two parameters. The parameter Φ characterizes the strength of the irregularities in terms of the correlation, $\rho(r, r')$, between the phase-speed fluctuations at different points on the unperturbed ray path:

$$\Phi^2 = k_o^2 \int_{ray} ds \int_{ray} ds' \, \rho(s,s') \quad , \tag{1}$$

where k_o is the free-space (electromagnetic) wave number and ds is an increment of distance along the ray. This expression constitutes a straightforward generalization of the expression that arises for a uniform background medium.

If the medium fluctuations decorrelate over a distance that is short compared with that over which the statistical inhomogeneity of the medium becomes evident, then Φ can be written in terms of the local mean-square refractive-index fluctuations, $\langle\mu^2(s)\rangle$, and a local integral scale, $L_p(s)$, that characterizes the spatial correlation of the fluctuations in the vicinity of s:

$$\Phi^2 = k_o^2 \int_{ray} ds \langle\mu^2(s)\rangle L_p(s) \quad . \tag{2}$$

For a horizontally stratified medium, with z vertical and thus perpendicular to the planes of stratification, the dependence on s is reduced to a dependence on z, and L_p can be written

$$L_p(z) = \frac{1}{\langle\mu^2(z)\rangle} \int_{-\infty}^{\infty} du \, \rho(u,\theta,\phi;z) \quad . \tag{3}$$

In Eq. (3), u is measured from s along the tangent line to the ray at s, at angle θ to the vertical, as is illustrated in Figure 1. The presence of θ and ϕ on the right side of Eq. (3) indicates that L_p depends on the direction of the path at s as well as on the local characteristics of the medium there. The dependence of L_p on the azimuthal angle ϕ is absent for the oceanic fluctuations treated by Flatté et al.[5]

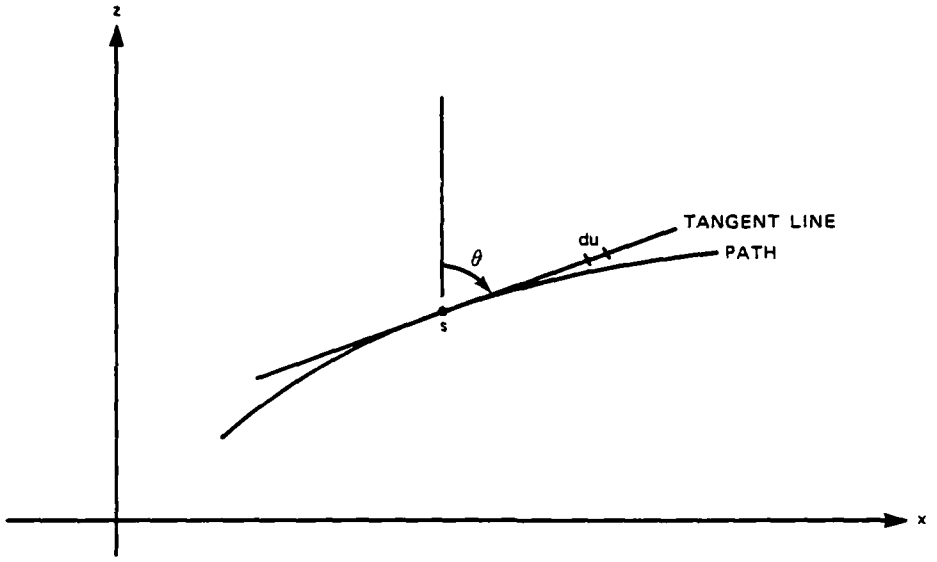

Figure 1. Tangent line integration for L_p

The diffraction parameter Λ characterizes the effects of the size of the fluctuations on the received signal:

$$\Lambda = \frac{k_o^2}{\Phi^2} \int_{ray} ds \langle \mu^2(s) \rangle L_p(s) \left[\frac{1}{|k_o A(s) L_v^2|} + \frac{x(R-x)}{k_o R L_h^2} \right] , \qquad (4)$$

where x is horizontal distance in the plane of the unperturbed ray and R is the horizontal distance between source and receiver. The scales L_v and L_h characterize the fluctuation correlations in the vertical plane and horizontally, respectively, transverse to the ray path. In contrast to the correlation length along the path, L_p, the scales L_v and L_h describe the differential variation of ρ in the two transverse directions. For a power-law irregularity spectrum, they are defined[6] as

$$\frac{1}{L_\perp^2} = \lim_{r \to o} \frac{\int d^2 k_t \Omega(o, k_t)[1 - \cos(k_t \cdot r)]}{\int d^2 k_t \Omega(o, k_t)} , \qquad (5)$$

where $\Omega(\underset{\sim}{k})$ is the irregularity wavenumber spectrum

$$\Omega(\underset{\sim}{k}) = \frac{\langle \mu^2 \rangle_c}{k^n} \tag{6}$$

with n the three dimensional spectral index.

The parameter A(s) that appears in Eq. (4) is termed the phase curvature. It is defined[5; Sec. 7.1] as the second derivative of the phase path length for a lateral displacement of the ray path from its nominal position. Thus, A is related to the Fresnel-zone radius, R_F, by $R_F = 2\pi(k_o A)^{-1}$. Note that A is a function of location along the ray path, as is R_F. In the case of a horizontally stratified medium, the phase curvature for horizontal displacements transverse to the path is the same as that for a straight-line path of the same length through a uniform medium[6]. For vertical displacements, however, the refractive bending of the ray path markedly affects the phase curvature. Additionally, consideration of vertical displacements in the vicinity of caustics of the ray path raises questions that involve the basic limitations of ray theory itself. The nature of these difficulties and their impact on calculation of the diffraction parameter is discussed in Section 3.

Evaluation of correlations between samples of the received signal additionally requires knowledge of the phase-structure function, D, which describes the difference in phase between two points separated in space, time, or frequency. In analogy with the definition of D for an homogeneous unperturbed medium, Flatté et al.[5] define this quantity as

$$D = \left\langle \left[k_{o_1} \int_{\text{ray } 1} ds_1 \, \mu(s_1) - k_{o_2} \int_{\text{ray } 2} ds_2 \, \mu(s_2) \right]^2 \right\rangle \quad . \tag{7}$$

As in the case of the strength parameter Φ, the generalization of the expression for D to a refractive background medium is nominally straightforward.

SECTION 3
EFFECTS OF CAUSTICS

In Section 2 we noted that the complexity of the unscattered field structure in the ionosphere causes some difficulties in the calculation of the diffraction parameter A. These difficulties result specifically from the presence of caustics in the unperturbed ray structure. Calculation of the diffraction parameter entails determination of the wave-field characteristics in the vicinity of the unscattered ray path. Flatté et al.[5] use ray expressions to describe these characteristics; their expressions fail when the unperturbed ray is near a caustic.

The ramifications of this complication can best be assessed in the context of an ionospheric model that has analytic expressions describing the unperturbed wave fields. A linear-gradient model of the variation of ionospheric electron density with height, although somewhat too idealized for practical application, serves this purpose well. This model will be described next, after which the nature of the fields near caustics will be examined. Modifications to the calculation of the diffraction parameter that account for the caustic effects will be described in the final portion of this section.

3.1 Linear-Gradient Profile Model

A linear-gradient model of ionospheric electron-density variation with height allows the field characteristics to be determined analytically. With this model the variation of the wave fields as a function of location can be examined to whatever degree of detail is required. Basic expressions for the ray paths and their phase-path lengths have been derived from the general formulas given by Budden.[8] With these, the phase-path length (i.e., the distance along a ray measured in wavelengths) to a scattering point can readily be found as a function of the position of this point. The full-wave characteristics of the field variations near caustics can also be determined relatively easily.

The linear-gradient electron-density profile takes the form

$$f_p^2 = \begin{cases} 0 & z < h_o \\ \alpha(z - h_o) & h_o < z \end{cases} , \tag{8}$$

where f_p is the plasma frequency, z the height, h_o the base height of the profile below which the medium is free space, and α the profile gradient parameter. Ray paths are described generally by

$$x = S \int_o^z \frac{dz'}{q} , \tag{9}$$

where x is the horizontal distance, and $S = \sin \Phi_I$ is the sine of the angle Φ_I between the wave-normal (and ray) direction and the vertical axis at the origin (x = 0, z = 0). The quantity q is the refractive-index parameter introduced by Booker.[9]

$$q = n \cos\theta = (n^2 - S^2)^{\frac{1}{2}} , \tag{10}$$

where $n = (1 - f_p^2/f^2)^{\frac{1}{2}}$ is the refractive index for frequency f. The earth's magnetic field has not been included in the refractive index expression because its effects are incidental to those of primary interest here.

The phase-path length along a ray from the origin (0,0) to the point (x,z) is given generally by

$$\varphi = k(x\, S + \int_o^z q\, dz') , \tag{11}$$

where $k = 2\pi f/c$ is the free-space wave number. The point (x,z) may be accessible along more than one ray. The phase-path length φ generally differs in this case for the different rays, as is implied by the presence in Eq. (11) of the parameter S, by which the rays are differentiated from one another.

The use of Eqs. (8) and (10) in Eq. (9) yields a specific description of the ray paths for this profile, namely,

$$x = \begin{cases} \dfrac{S}{C} z & z \le h_o \\ \dfrac{S}{C} h_o + 2\dfrac{f^2}{\alpha} S\left\{C - \left[C^2 - \dfrac{\alpha(z-h_o)}{f^2}\right]^{\frac{1}{2}}\right\} & h_o \le z \end{cases} \Bigg\} x \le \frac{D}{2}$$

$$\Bigg\{ \begin{cases} \dfrac{S}{C} h_o + 2\dfrac{f^2}{\alpha} S\left\{C + \left[C^2 - \dfrac{\alpha(z-h_o)}{f^2}\right]^{\frac{1}{2}}\right\} & h_o \le z \\ (2h_o - z)\dfrac{S}{C} + 4\dfrac{f^2}{\alpha} SC & z \le h_o \end{cases} \Bigg\} \frac{D}{2} \le x \qquad (12)$$

where $C = \cos \Phi_I$ and

$$D = 2\frac{S}{C} h_o + 4\frac{f^2}{\alpha} SC \qquad (13)$$

is the distance between the ground-intersection points (0,0) and (D,0) of the ray. A set of paths calculated using Eq. (12) for a frequency of 5 MHz, with h_o = 100 km and α = 0.1 MHz^2/km, is shown in Figure 2. In this example, rays have been launched at 5° increments at angles between 5° and 85°.

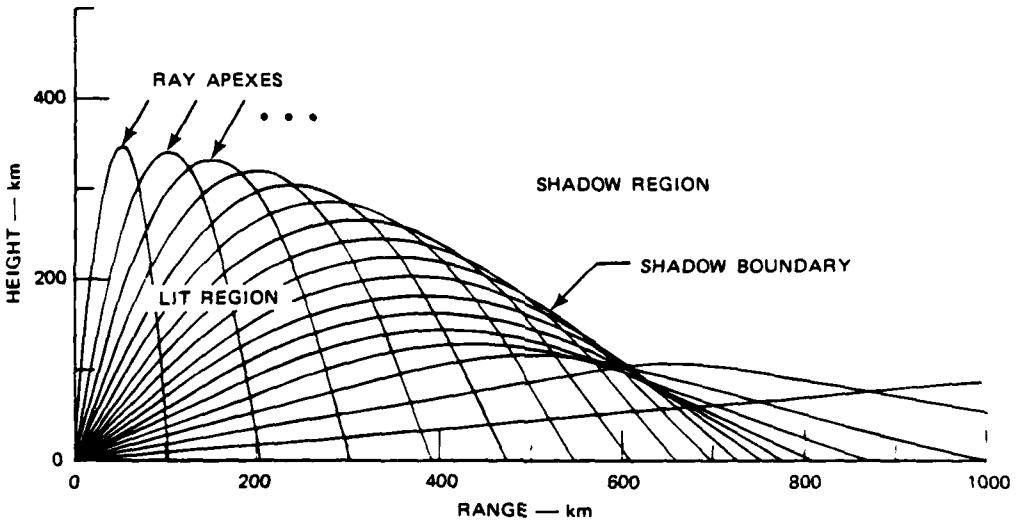

Figure 2. Ray paths for linear electron-density gradients

According to Eq. (8), the ray paths within the ionosphere are sections of parabolas; beneath the ionosphere, of course, they are sections of straight lines. Any point beneath the ionosphere is connected to the source by two rays. One of these is the straight, line-of-sight ray beneath the ionosphere; the other ray is that reflected from the ionosphere by the process of refraction. There is a skip zone for frequencies sufficiently high to penetrate the ionosphere at steep angles of incidence. This phenomenon is absent for the linear-gradient ionospheric model because the electron density in this model increases without limit with increasing height in the ionosphere.

Within the ionosphere, a shadow boundary, or ray caustic, exists above which no rays penetrate. The location of this boundary, which is evident in Figure 2, is frequency dependent. At any point below the shadow boundary, as beneath the ionosphere, at least two rays can generally be found to connect a given point with the source. The existence of at least two rays can be deduced qualitatively by considering the evolution of the line of sight and the ionospherically refracted rays as a receiver is moved up into the ionosphere from beneath it. The two rays ultimately coalesce at the caustic. Near the caustic, as can be seen in Figure 2, one of the rays, the one with the steeper launch angle, has already touched the caustic at a slightly shorter range, while the other ray is about to reach the caustic at a slightly greater range.

This circumstance has implications for scatter; multiple ray paths must be considered between the scatter location and both the source and the receiver locations. These paths are illustrated schematically in Figure 3 for a scatter point at an arbitrary point on unscattered ray path. If the two possible ray paths between the scatter point and the source, or the receiver, constitute distinct rays (a condition that can be given precise meaning), then only one of them, the one directly evolvable from the unperturbed ray path between source and receiver, is important. Near a caustic, however, the two rays are not distinct; indeed, a ray description of the field behavior near the caustic fails for just this reason.

The theory developed by Flatté et al.,[5] which uses ray expressions to describe the fields everywhere, fails to address the above situation.

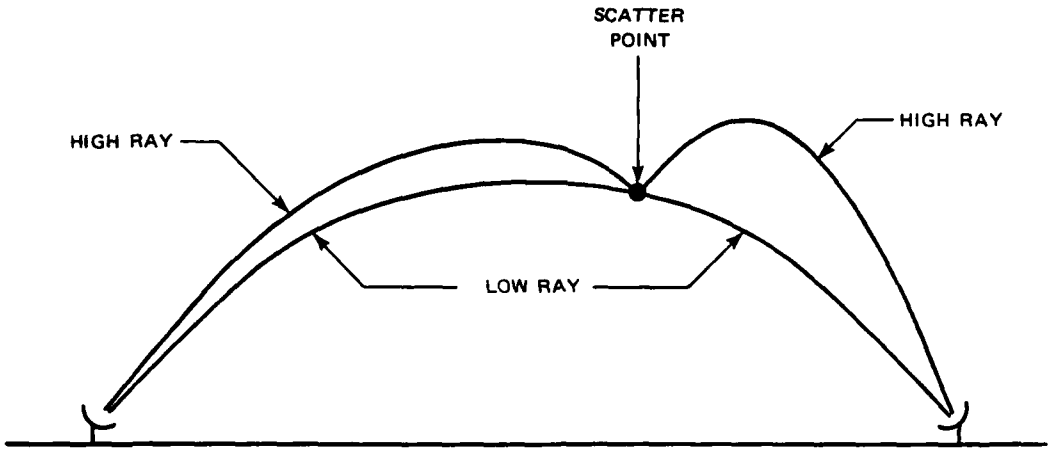

Figure 3. Multiple rays joining point to path endpoints

The hope, of course, is that a precise treatment of shadow boundaries formed by caustics will not prove to be critical. This expectation is reasonable, given the general success of Kirchoff approximations in the treatment of large diffracting objects, but such a result should not be presumed without inquiry.

Determination of the locations of the apex and caustic surfaces for an ensemble of rays facilitates iteratively selecting the appropriate ray to reach a particular point. This procedure will be used to examine the rate of variation of some path parameters with displacement of a scattering point transverse to the ray path.

For our linear-gradient model, the apex of a ray represents an extremum of the height, z, as a function of the distance, x, as the ray is traced. This extremum is simply identified in the equations for the ray paths, [Eq. (12)]. A ray, according to Eq. (12), reaches its apex at $x = D/2$, where the radical in the expressions valid for $z \geq h_o$ becomes zero, giving

$$x_a = \frac{S}{C} h_o + 2\frac{f^2}{\alpha} SC \qquad (14a)$$

$$z_a = h_o + \frac{f^2}{\alpha} C^2 \qquad (14b)$$

for the apex coordinates (x_a, z_a) as a function of θ_I. A plot of $z_a(x_a)$ is shown in Figure 4 for the set of rays traced in Figure 2 for $f = 5$ MHz, $h_o = 100$ km, and $\alpha = 0.1$ MHz^2/km.

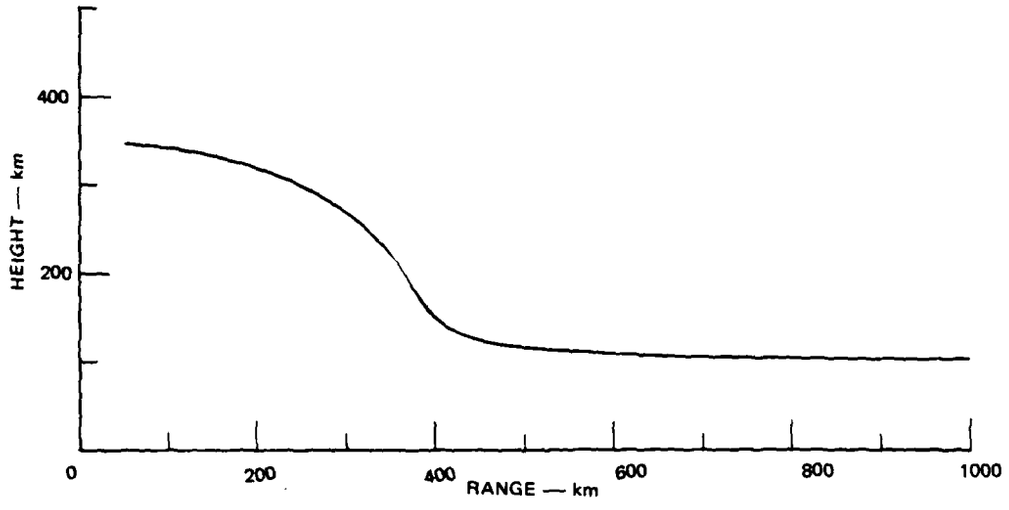

Figure 4. Locus of apexes for rays traced through linear-gradient electron-density profile

Determination of the location of the caustic surface is somewhat more complicated. A caustic surface can be defined as the locus of points (x_c, z_c) for which the rate at which a ray is shifted laterally (transverse to itself) by a change in its launch angle, θ_I, is zero. The location of this surface can most simply be determined for the linear-gradient profile through the setting to zero of the partial derivative $\partial x/\partial\theta_I$ with z held fixed, with the result

$$x_c = \begin{cases} \dfrac{8f^2}{\alpha} S^3 C & z_c \leq h_o \\ \dfrac{S}{C} h_o + 2\dfrac{f^2}{\alpha} S \left\{ C + \dfrac{\left[\left(C^2 - S^2 + \dfrac{\alpha h_o}{2f^2C^2}\right)^2 + 4S^2C^2\right]^{\frac{1}{2}} - \left(C^2 - S^2 + \dfrac{\alpha h_o}{2f^2C^2}\right)}{2C} \right\} & h_o \leq z_c \end{cases} \quad (15a)$$

$$z_c = \begin{cases} 2h_o - \dfrac{4f^2}{\alpha} C^2 (S^2 - C^2) & z_c \leq h_o \\ h_o + \dfrac{f^2}{\alpha} \left\{ C^2 - \dfrac{\left\{\left[\left(C^2 - S^2 + \dfrac{\alpha h_o}{2f^2C^2}\right)^2 + 4S^2C^2\right]^{\frac{1}{2}} - \left(C^2 - S^2 + \dfrac{h_o}{2f^2C^2}\right)^2\right\}^2}{4C^2} \right\} & h_o \leq z_c \end{cases} \quad (15b)$$

for the caustic coordinates (x_c, z_c) as a function of θ_I.

A plot of $z_c(x_c)$ is shown in Figure 5 for the ray set traced in Figure 2.

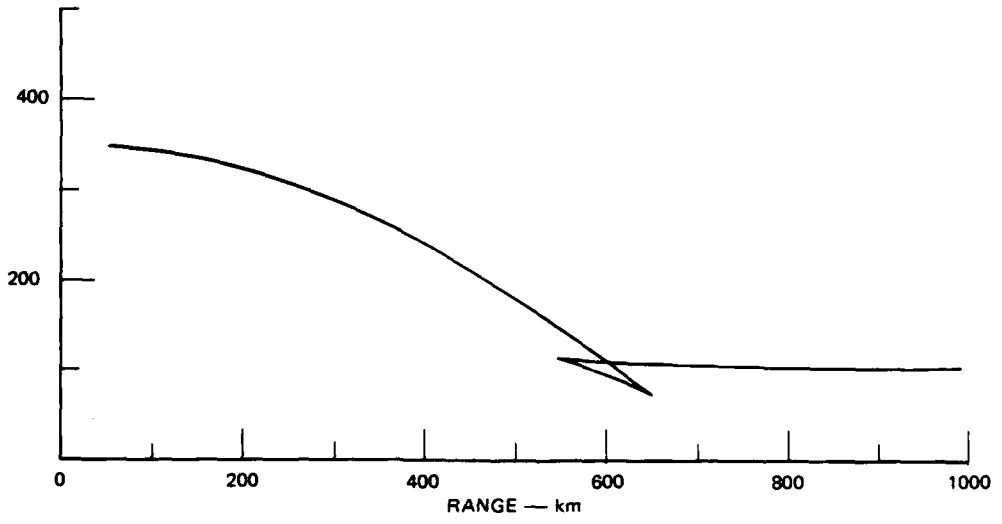

Figure 5. Caustic surface for rays traced through linear-gradient electron-density profile

3.2 Field Structure near Caustics

Expressions were given in Section 3.1 for finding ray paths and the phase-path length along these paths from a localized source to an arbitrary point. These expressions can be obtained by stationary-phase evaluation of Fourier-transform integrals that relate the individual plane-wave (angular spectrum) components of the field to its spatial variation.[8] For a plane-stratified background medium like the linear-gradient ionospheric profile employed here, this procedure is quite effective and yields as well the standard ray-optics expressions for the field amplitude. As already noted, these expressions are not valid in the vicinity of caustics. In the context of an angular-spectral field representation, each ray is associated with a distinct saddle point across which the path of the transform integration passes. The coalescence of rays that forms a caustic is thus expressed as a merging of two saddle points, and the stationary-phase technique for approximating the integral across the saddle as an asymptotic series fails. The variation of field intensity near caustics was first determined by Airy;[10] the characteristics of this variation are discussed in sufficient detail for our needs by Budden in Section 11.7.

The variation of the field-intensity, I, transverse to the caustic surface is given by

$$I = Ai\left[u\left(\frac{2k^2}{R}\right)^{1/3}\right] \quad , \tag{16}$$

where Ai is the Airy integral function, u is the perpendicular distance from the caustic, k is the local wave number in the medium, and R is the radius of curvature of the caustic. Equation (16) can be expressed in terms of the local refractive index and the launch angle of the ray that touches the caustic at u = o through use of Eq. (10). The curvature R can also be expressed in terms of these quantities and the rate at which this ray moves as the launch angle is changed by noting that R is given by

$$R = \left[\frac{d^2x}{d\theta^2}\ \cos\theta\right]_{\theta=\theta_o} \quad , \tag{17}$$

where θ_o is the local angle of the ray at u=0. Expression of R in terms of a derivative of x with respect to the angle θ is convenient in light of the explicit dependence of x on θ given for the linear-gradient profile by Eq. (12).

Use of Eq. (17) in Eq. (16) with Eq. (10) employed to express the local wave number k in terms of the free-space wave number k_o through $k = nk_o$, yields

$$I = Ai\left\{nu\left[\frac{2k_o^2 \cos^2 \theta_{I_o}}{\left(n^2 - \sin^2\theta_{I_o}\right)^{3/2} d^2x \left|d\theta^2\right|_{\theta_I = \theta_{I_o}}}\right]^{1/3}\right\} \qquad (18)$$

The form of the field behavior near the caustic is shown in Figure 6, in which the behavior of the Airy function is shown as a function of

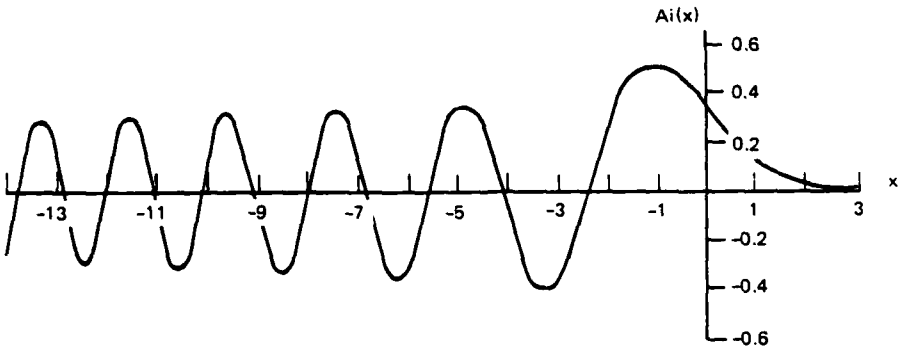

Figure 6. The airy integral function Ai(x)

the value of its argument. For negative values of the argument, the function is oscillatory. If the Airy function is expressed as an integral, the integral can be well approximated by stationary-phase evaluation at the saddle points on the integration path for sufficiently large values of the Airy-function argument. For large negative values of the argument, this path crosses two saddle points, and the oscillatory behavior of the function can be interpreted as showing interference between two rays, as their relative phase changes, on the illuminated side of the caustic. For large positive values of its argument, the Airy function decays

exponentially, showing the transition into the shadow on the other side of the caustic.

3.3 Evaluation of the Diffraction Parameter

In Section 3.1 we showed that the ensemble of ionospheric ray paths forms caustic surfaces. Ray concepts fail to describe the field behavior near these caustics. Thus the presence of caustics in regions of appreciable scatter can greatly complicate attempts to calculate scatter effects using a purely ray treatment. In particular, the phase curvature for displacements in the plane of the unperturbed ray path is discontinuous at caustics, as will be demonstrated. The effects of this discontinuity on the integral for the diffraction parameter [Eq. (4)] is assessed in this section.

The phase curvature is defined[5] as the second derivative of the phase-path length with respect to lateral displacements of the path, such as that shown in Figure 7. In a horizontally stratified, isotropic

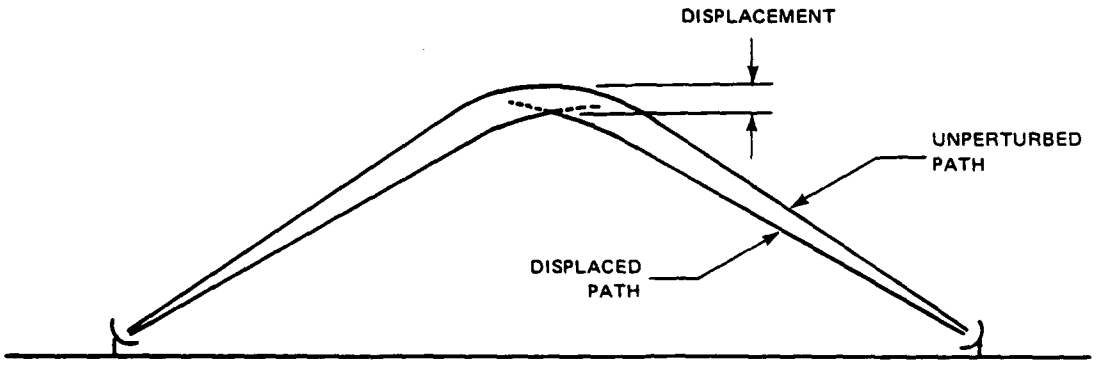

Figure 7. Lateral displacement of ray path vertically

medium (e.g., to first approximation, the ionosphere), horizontal displacements yield results similar to those for a homogeneous medium. However, displacements in the plane of the ray path lead to more complex results because they involve the phenomena responsible for the ray refraction.

If the phase-path length is calculated for vertical displacement of the ray path as a function of the extent of the displacement, the result varies as the location changes on the path from which the displacement is made. The results of several such calculations are shown in Figure 8 for vertical displacements at a series of locations along the ray path that are offset horizontally from the apex by multiples of 2 km, starting at 0 km [Figure 8(a)]. The phase curvature for a given vertical displacement is the inverse of the radius of curvature of the curves plotted in Figure 8. The unperturbed ray path in these examples is one of the ray set shown in Figure 2 for a linear-gradient electron-density profile and a 5-MHz frequency. The takeoff angle of the unperturbed ray was adjusted to a value that gave a total path length of 1500 km.

The phase-path lengths shown in Figure 8 for the perturbed ray paths were calculated as the sum of those for the two ray segments that join the displaced path point to the two (fixed) endpoints of the path. The existence of multiple phase-path lengths for a given displacement (i.e., the existence of several curves in each of the figures) results from the presence of more than one ray path between the displaced path point and one or both of the path endpoints. Away from caustics, only one pair of these paths evolves into the unperturbed ray path as the vertical displacement is reduced to zero. This unperturbed ray is found at the point of zero slope in the variation of phase-path length with vertical displacement. The phase curvature used to determine the diffraction parameter A is given by the radius of curvature at this point.

At the ray apex, Figure 8(a), the unperturbed ray is found on the lowest of the three curves, where the phase-path length attains a maximum. The other two curves result from a second, higher ray on one (middle curve) or both (upper curve) path segments, as is illustrated schematically in Figure 3 for a point somewhat to one side of the ray apex. (The presence of multiple rays to points on a ray path can also be seen in the ray set shown in Figure 2.) As the path is displaced upward, the separation between the higher and the lower rays decreases until the rays coalesce into a single ray at a caustic. The approach to the caustic is shown in Figure 8(a) by the decrease in the difference in

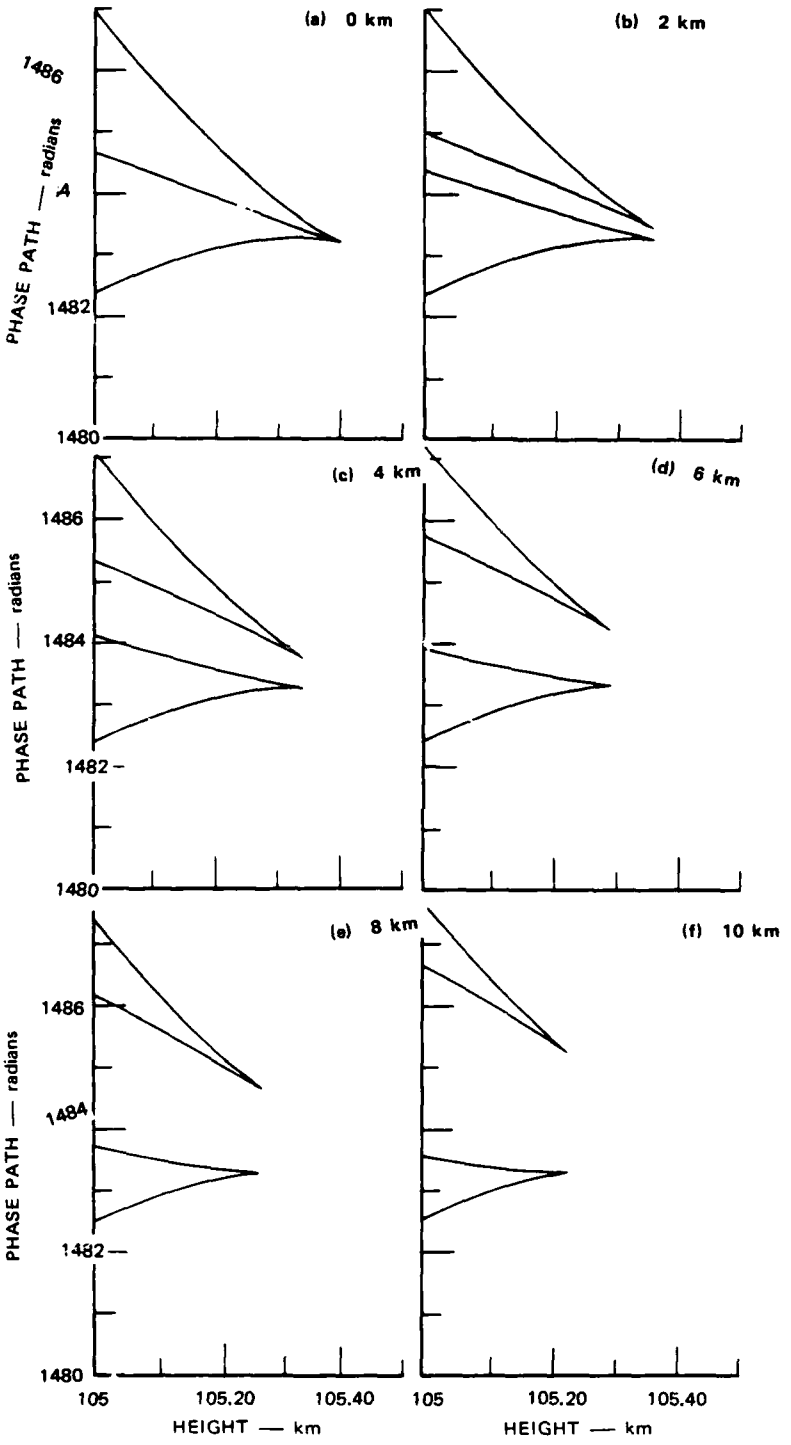

Figure 8. Phase-path lengths as a function of bertical displacement at various points along a ray path

phase-path length among the three curves as height increases; the curves join at the caustic height.

Figure 5, introduced previously, shows the caustic surface pertinent to the ray set at hand here. A second caustic surface, that for the path with the source and receiver reversed, also is pertinent. This surface can be found by mirroring the first caustic surface in a vertical line through the path midpoint. The two caustic surfaces thus intersect above the path apex.

For points on the ray path horizontally to either side of its apex, Figures 8(b) to 8(f), the middle curve of Figure 8(a) has split into two curves. This split results from the asymmetry between the two sections of the path, which no longer traverse equal horizontal distances. For small horizontal offsets, the form of the variation in phase path length as the vertical displacement changes otherwise is generally similar to that found at the path midpoint. As the horizontal offset is increased, however, a caustic is approached on the ray path, and the junction point of the lower curve pair moves nearer the position of the undisplaced ray on the lowest curve [Figures 8(d) and 8(e)]. As the horizontal offset is further increased so that the caustic is passed [Figure 8(f)] the unperturbed ray shifts to the upper curve of this pair, with an attendant reversal in sign of the phase curvature. This sequence is shown more clearly in Figure 9, where the variation of phase path length with vertical displacement for the lower curve pairs of Figure 8 are plotted to a slightly different scale at 5-km increments in horizontal offset.

The variation of the phase curvature along the unperturbed ray for a path of about 1000-km total length is shown in Figure 10. The location on the ray path of the caustic responsible for the discontinuity evident in the curvature at about 450 km is shown by the cross mark in Figure 11. Only one half of the ray path is shown. The ray traced in this figure again is one (that launched at an angle of 75° with respect to the zenith) of the set shown in Figure 2.

These results suggest that the phase-path length might generally be considered to be a multivalued function of the position of a point joining

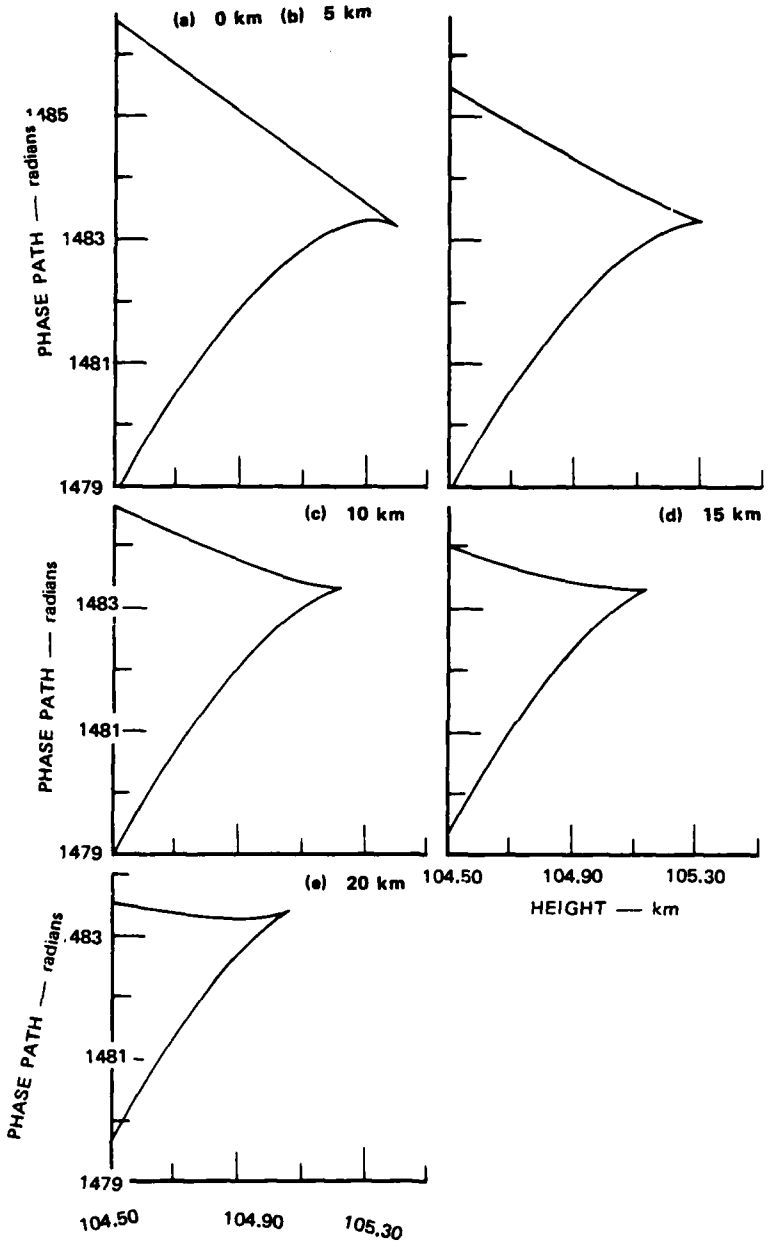

Figure 9. Phase-path lengths as a function of vertical displacement at path points near a caustic

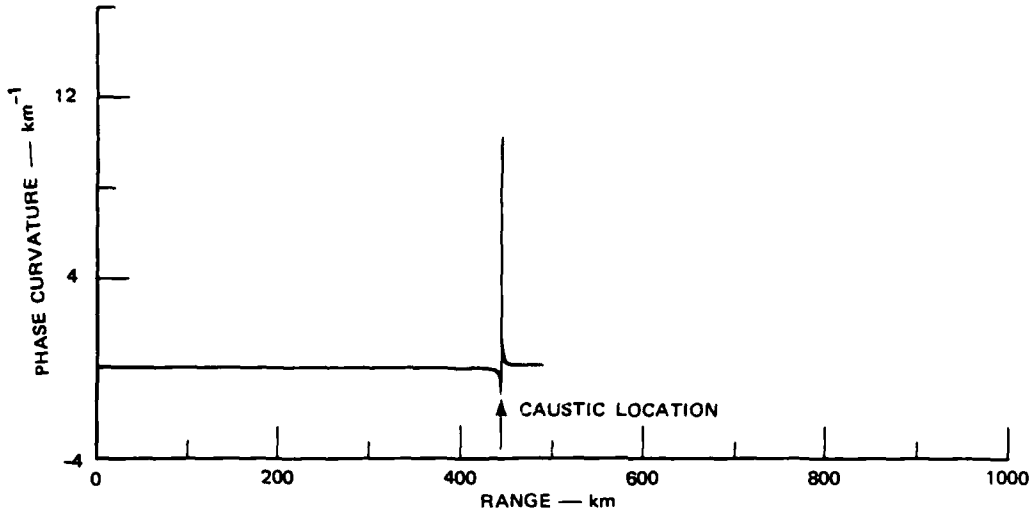

Figure 10. Phase curvature as a function of position along a ray

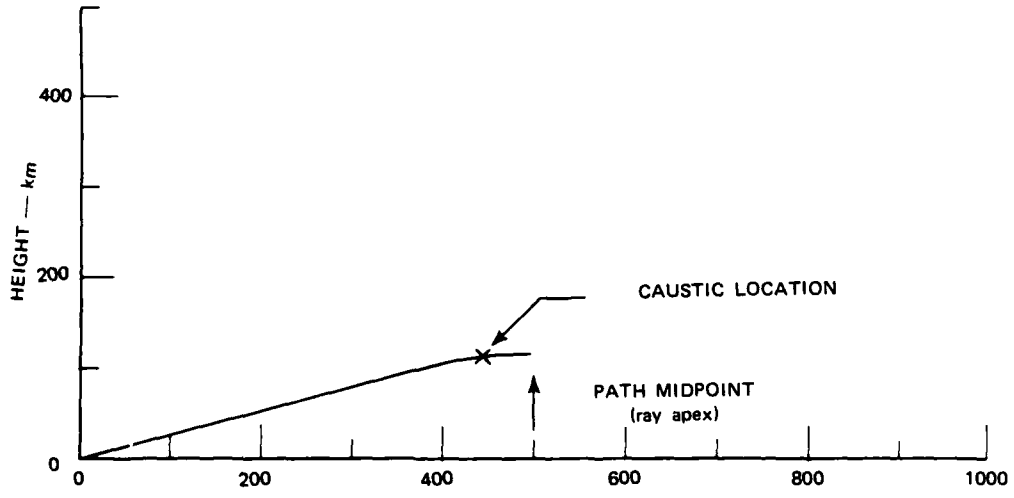

Figure 11. Location of caustic on ray with 75° launch angle

rays to fixed path endpoints. The multivaluedness represents the multiplicity of rays that are possible for each of the path's two segments. At caustics, two branches of the phase-path curve join as two rays coalesce. The shift of the phase extremum associated with the total-path ray from one to the other of these two branches as the caustic is passed causes the phase curvature to change discontinuously, with a change of sign, across the caustic.

This multiplicity of ray paths is of little consequence for scatter points that are well removed from caustics; only that pair of path-segment rays that constitutes a valid ray for the entire path needs to be considered. For this valid ray, the phase curvature provides a useful estimate of the Fresnel-zone size, which in turn determines the distance to either side of the ray over which fluctuations of the medium must be correlated for diffractive effects not to become significant. Other combinations of segment rays lack the extremum of phase associated with a first-order contribution to the field at the receiver.

At points near a caustic, however, the two coalescing rays are no longer distinct entities, and the field behavior is not well represented in terms of rays at all. The Airy integral function introduced in Section 3.2 provides a better description of the fields in such regions, showing the interference between the two rays on the lighted side of the caustic, the transition into the shadow, and the decay of the field in the shadow region. Thus, it is appropriate to seek a meaningful length scale based on this description.

Clearly, refractive-index fluctuations well within the shadow region should not affect the received field. The rate at which the field decays as the shadow region is entered is described by the Airy function; this rate provides a natural length scale for diffraction near the caustic. This characteristic length is similar to the distance on the opposite (lighted) side of the caustic required for the difference in phase between the two rays to become equal to π radians (cf. Figure 6). Since the ray joining the perturbed path point to the receiver is common to both rays, this latter distance is also that over which the difference

in total phase-path length for the two rays becomes π radians (as seen, for example, in Figure 9).

Although not zero at the caustic (as is the scale derived from the phase curvature), the characteristic length suggested by the Airy-function behavior remains small relative to the size, at points well removed from the caustic, of a Fresnel zone. The contribution to the diffraction integral, Eq. (4), from fluctuations of refractive index in the plane of the ray path near the caustic consequently would appear to be minimal, as has previously been assumed.[6] Thus, a precise treatment of the caustic region should be unnecessary, and use of the phase curvature throughout the diffraction integral would not be expected to introduce substantial errors.

The Fresnel-zone radius given by the phase curvature of Figure 9 is shown in Figure 12 as R_v. The Fresnel-zone radius in the horizontal direction, given by $x(R-x)/k_oR$, is also shown for comparison as R_h.

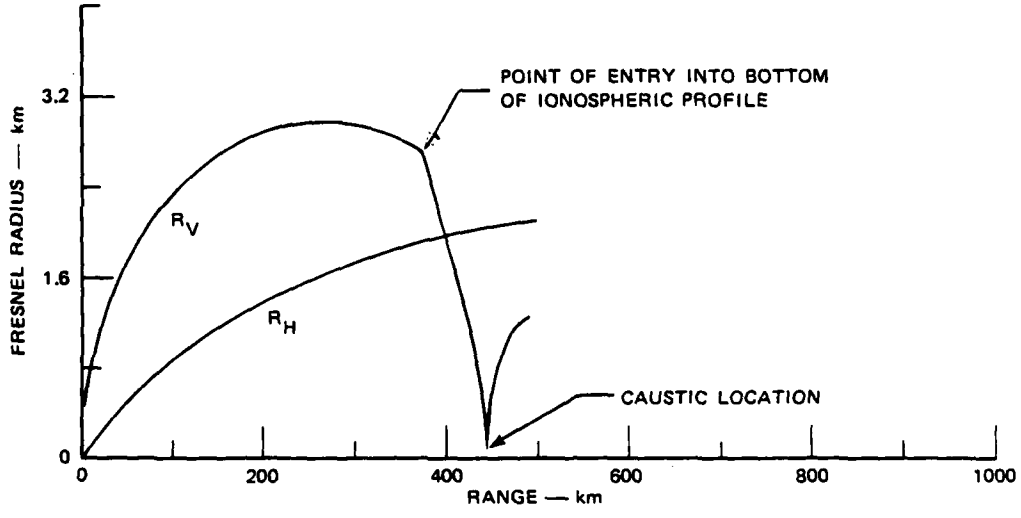

Figure 12. Fresnel-zone radius prodicted by phase curvature as a function of position along a ray

Between the caustics, the zone size in the vertical direction is seen to remain smaller than that in the horizontal direction. The diffraction

contribution from fluctuations in the horizontal direction thus tends to dominate for equal transverse scale sizes vertically and horizontally.

SECTION 4
APEX APPROXIMATION

The effects of small-angle forward scatter, resulting from stochastic irregularities of the propagation medium, on signals that also are refracted by large-scale, deterministic variations in the medium can, according to Flatté et al.,[5] be described to a good approximation in terms of integrals of various quantities taken along the mean (effectively, unscattered) ray path. In these circumstances, the intensity of the smaller-scale random fluctuations in refractive index that scatter the signal may be related in some manner to the deterministic refractive-index variations. For example, the rms magnitude of the smaller scale electron-density fluctuations in the ionosphere can in many cases be approximated as being some constant fraction of the mean electron density at each point.

A further approximation to the path integrals, termed the apex approximation, has been proposed by Flatté et al.[5, Chapter 11] for cases where the scatter effects are concentrated, as in the above example, near the apex of the ray path. In this approximation, the random phase perturbations accumulated along the ray path are applied to the wavefront in a single lumped increment, as the ray passes through a plane placed transverse to the path at the path apex, or turning point. The perturbed field can then be treated as a secondary source, in accordance with Huygen's principle, to calculate the received wavefield including scatter. Thus, the apex approximation constitutes a generalization to refracted ray paths of the thin-phase-screen approximation.

Flatté et al.[5, Sec. 11.1] note that the validity of this approximation requires, in addition to the scatter being concentrated near the path apex, that the wave intensity in the vicinity of the apex not be much affected by the scatter and that the phase modulation of the wave be calculable using geometrical optics. They further observe that these requirements generally are met if propagation remains in the geometrical-optics regime over a sufficient horizontal distance about the apex, namely

$(r \times L_V)^{1/2}$, where r is the ray radius of curvature at the apex and L_V is the vertical scale of the irregularities, defined in Section 2. This condition implies that caustics must not be encountered along the ray path within this distance since geometrical optics is fundamentally incapable of describing the wavefield behavior in the vicinity of a caustic.

Another way to understand this constraint is to consider the apex approximation as an expansion about the path apex of the parameters that are integrated along the path to describe the scatter effects. In order for this expansion to be useful, it must be valid for the entire portion of the path over which appreciable scatter occurs. As was shown in Section 3.3, however, the phase curvature is rather ill behaved near caustics. This behavior essentially limits the range about the path apex over which the phase curvature and related quantities can be expanded.

The results obtained in Section 3 provide some indication of the potential usefulness of the apex approximation at HF. Comparison of the caustic surface for the ray set, Figure 5, with the apex surface, Figure 4, reveals that these surfaces are not greatly separated in two regions, namely for values of x less than about 300 km and greater than about 600 km, corresponding to rays with very steep or very shallow take-off angles, respectively. This behavior suggests that for these rays the caustic and apex locations may not be sufficiently separated to allow the use of the apex approximation.

The horizontal distance between the caustic and the apex can be explicitly calculated using Eqs. (14a) and (15a) to determine x_a and x_c, respectively. The result of this calculation for the set of rays presented in Figure 2 is shown in Figure 13. Calculation of the radius of curvature, r, of the ray path for a linear-gradient electron-density profile gives

$$r = \frac{2f^2S^2}{\alpha} \tag{19}$$

at the path apex. Evaluation of Eq. (19) as a function of $S = \sin \theta_I$, together with a nominal value of 10 km for L_V, yields the second curve shown in Figure 13. Comparison of the two curves confirms that, for both

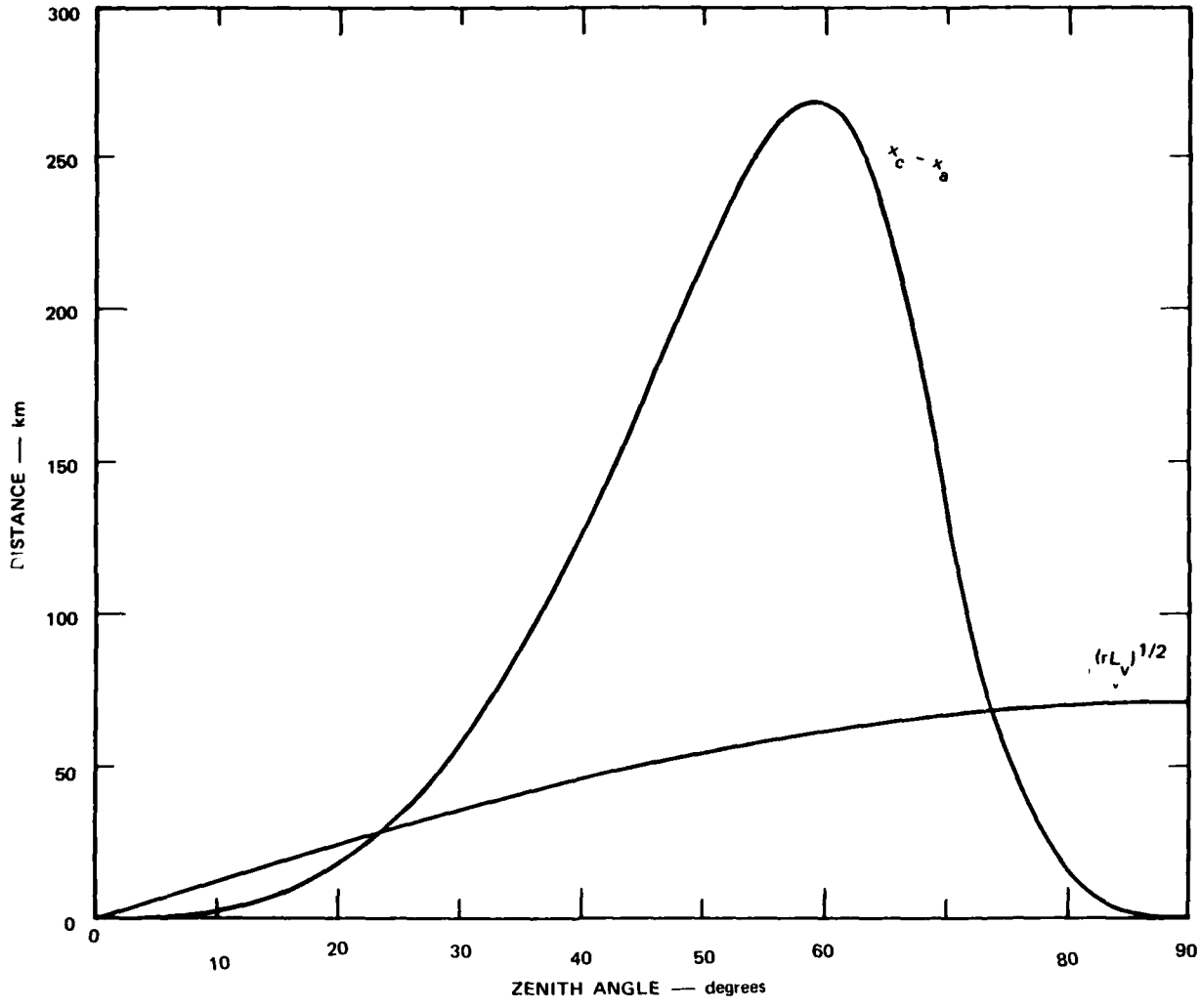

Figure 13. Comparison of caustic/apex separation with apex-approximation criterion

the very steep ($\theta_I < 25°$) and the very shallow ($\theta_I > 75°$) rays, the separation of the path apex and the caustic is less than $(r \times L_V)^{1/2}$ and therefore, according to the criterion reiterated above, indeed too small for the apex approximation to be valid.

Although the linear-gradient profile used in this example differs significantly from actual ionospheric profiles in some of its characteristics, the shallow rays are representative of the propagation behavior, on long HF paths, of frequencies below the maximum usable frequency. Thus, it is necessary to conclude that the utility of the apex approximation may be somewhat limited at HF. The steep-incidence rays, although representative of the behavior on a short path of frequencies below the vertical-incidence critical frequency, are less instructive; they represent a case for which the basic applicability of the path-integral scatter theory can be questioned more generally. Namely, it is difficult to view the electron-density fluctuations as leading only to small-angle scatter in this case since the signal frequency approaches the plasma frequency near the path apex, and the fluctuations consequently strongly perturb the height at which the plasma is overdense at the wave frequency.

SECTION 5
CHANNEL-PROBE PARAMETERS

An experiment has been planned[2] to measure the impulse response (i.e., the time-delay and Doppler spread of the received signal for an impulsive source) of an HF channel. This measurement suffices to characterize the channel completely in the absence of spatial diversity. The theory discussed in preceeding sections of this report characterizes the impulse response of the channel in terms of two parameters, the coherent bandwidth and the coherence time, that are closely related to the parameters that are measured experimentally.

The coherent bandwidth, (η_w) is given by[5, §8.6]

$$\eta_w = \frac{\pi^2}{6}\,\omega\,\left(\Lambda\Phi^2 \mathrm{in}\Phi\right)^{-1} \tag{20}$$

in the fully saturated case, neglecting a factor of order unity that involves the ratio of a scale for variation of the phase-structure function to that for the refractive-index fluctuations. The delay spread (T_D) measured experimentally is related to this bandwidth by

$$T_D = \frac{2\pi}{\eta_w} \quad . \tag{21}$$

The coherence time characterizes the correlation over time of the signal envelope fluctuations. The latter is given by[5, §8.4]

$$\langle \Psi^*(t+\Delta t)\Psi(t)\rangle = \exp\left[-\tfrac{1}{2}D(\Delta t)\right] \quad , \tag{22}$$

where $\Psi(t)$ is the (complex) signal envelope amplitude (also called the reduced wavefunction) at time t and D is the phase-structure function defined by Eq. (3). Generally, the phase-structure function for small time separations can be written[5, §7.5] in terms of the rate of change

of the strength parameter Φ as

$$D(\Delta t) = (\Delta t)^2 \dot{\Phi}^2 \quad , \tag{23}$$

although for small spectral-index values this quadratic approximation can break down.

In the case of HF ionospheric propagation, $\dot{\Phi}$ usually is considered to be determined by convection of irregularities across the ray path. In this case,[6]

$$D(\Delta t) \approx \tfrac{1}{2}\Phi^2 \left(\frac{v\Delta t}{L_h}\right)^2 \quad , \tag{24}$$

and the coherence time, T_c, is

$$T_c = \frac{2L_h}{v\Phi} \quad , \tag{25}$$

where v is the convective speed of ionospheric winds transverse to the path.

Experimentally, the coherence time is determined by measuring the time variation of a CW signal. The result of this measurement usually is transformed to yield a Doppler spectrum. The Doppler-spread parameter ω_D that characterizes the width of this spectrum is related to the coherence time by

$$T_c = \frac{2\pi}{\omega_D} \quad . \tag{26}$$

SECTION 6
CONCLUSIONS AND RECOMMENDATIONS

The path-integral theory developed by Flatté et al.[5] to describe scatter effects in the presence of deterministic refraction should be a useful tool in HF radiowave applications. A major simplification is achieved in their work by the approximation of the path-integral expressions by integrals taken along the unscattered ray path. We have examined carefully the effects on these expressions of caustics encountered midway along a ray path, which the theory as presented by Flatté et al. does not address. (Flatté et al. do note, however, that their results are not valid if the receiver is located near a caustic, such as would be the case for an HF receiver that happened to be near the skip distance.) Our examination found caustics encountered in midpath not to have much impact on the scatter behavior. Thus the inclusion of their effects, although fundamentally correct, would represent an unnecessary elaboration.

The apex approximation, which reduces the calculation of scatter effects on a strongly refracted ray path to a thin-phase-screen model, constitutes a further simplification of the path-integral theory. This simplification is possible only if caustics encountered along the path are sufficiently removed from the path apex. Our comparison, for a specific example, of the separation between caustic and apex with the minimum distance necessary to permit use of the apex approximation found this condition not to be met for a significant range of ray take-off angles. Although our results constitute only a single example, they suggest that the apex approximation should be used cautiously at HF.

As was noted in the introduction to this report, the linear-gradient ionospheric model used in this work falls somewhat short of the degree of realism desired for practical use. A better ionospheric model, which still retains the advantage of yielding explicit analytic expressions for the unscattered ray path, is that of a parabolic variation of electron density with height. This model probably represents the simplest that

should be considered for practical application. We recommend that the path-integral scatter theory, as reduced by Flatté et al.[5] to ray-path integrations, be implemented using this ionospheric model. In this implementation expressions for the basic channel parameters should be developed specifically for the HF application. Any need for further elaboration of the theory (including the consideration of more elaborate ionospheric models) can better be addressed after results obtained from the theory in this form have been compared with data from a field experiment, such as that described in the companion report[2] prepared under this contract.

LIST OF REFERENCES

1. E. T. Pierce et al., "The Global Ionospheric Effects of Nuclear Explosions. Part II: Observations," Final Report, Contract AF33(657)-12514, Stanford Research Institute, Menlo Park, California (June 1965).

2. R. P. Basler, "Experiment Plan for HF Channel Definition," Technical Report, Contract DNA001-82-C-0218, SRI Project 4571, SRI International, Menlo Park, California (February 1983). (In review.)

3. M. L. V. Pitteway, "The Reflection of Radio Waves from an Irregular Ionosphere," Tech. Report 382, Research Laboratory of Electronics, Massachusetts Institute of Technology, Cambridge, Massachusetts (November 8, 1960).

4. G. H. Price, W. G. Chesnut, and A. Burns, "Monopulse Radar Propagation through Thick, Structured Ionization," DNA 2907T, Special Report 4, Contract DASA01-69-C-0126, SRI Project 8047, Stanford Research Institute, Menlo Park, California (April 1972).

5. S. M. Flatté, R. Dashen, W. H. Munk, K. M. Watson, and F. Zachariasen, Sound Transmission Through a Fluctuating Ocean (Cambridge University Press, Cambridge, 1979).

6. M. Cornwall, S. Flatté, D. Hammer, and J. Vesecky, "Studies of the Effect of Striations on Radio Communications," JASON Tech. Report JSR-81-31, SRI International, Arlington, Virginia (December 1981).

7. L. A. Wittwer, "Radio Wave Propagation in Structured Ionization for Satellite Applications," DNA 5304D, In-House Report, Defense Nuclear Agency, Washington, D.C. (31 December 1979).

8. K. G. Budden, Radio Waves in the Ionosphere, Ch. 11, (Cambridge University Press, Cambridge, 1961).

9. H. G. Booker, "Oblique Propagation of Electromagnetic Waves in a Slowly-Varying Non-Isotropic Medium," Proc. Roy. Soc. A, Vol. 155, p. 235 (1936).

10. G. B. Airy, "On the Intensity of Light in the Neighborhood of a Caustic," Trans. Camb. Phil. Soc., Vol. 6, pp. 379-402 (1838).

DISTRIBUTION LIST

DEPARTMENT OF DEFENSE

Command & Control Sys Organization
ATTN: G500, R. Crawford
ATTN: G510, G. Jones
ATTN: G510, P. Bird

Defense Advanced Rsch Proj Agency
ATTN: GSD, R. Alewine
ATTN: T. Tether

Defense Communications Agency
ATTN: Code 230
ATTN: J300 for Yen-Sun Fu

Defense Communications Engineer Center
ATTN: Code R123, Tech Lib
ATTN: Code R410, N. Jones

Defense Intelligence Agency
ATTN: DB, A. Wise
ATTN: DB-4C
ATTN: DC-7B
ATTN: Dir
ATTN: DT-1B
ATTN: RTS-2B

Defense Nuclear Agency
ATTN: NATF
ATTN: NAWE
ATTN: RAAE, P. Lunn
ATTN: RAEE
ATTN: STNA
3 cy ATTN: RAAE
4 cy ATTN: STTI-CA

Defense Technical Information Center
12 cy ATTN: DD

Dep Under Secy of Defense, Cmd, Contl, Comm & Intell
ATTN: DADSD(I)
ATTN: Dir of Intelligence Sys

Field Command, DNA, Det 2
Lawrence Livermore National Lab
ATTN: FC-1

Field Command, Defense Nuclear Agency
ATTN: FCPR
ATTN: FCTT, W. Summa
ATTN: FCTXE

Interservice Nuclear Weapons School
ATTN: TTV

Joint Chiefs of Staff
ATTN: C3S
ATTN: C3S Evaluation Office, HDOO

Joint Data System Support Ctr
ATTN: C-312, R. Mason

Joint Strat Tgt Planning Staff
ATTN: JLK, DNA Rep
ATTN: JLKS
ATTN: JPPFD
ATTN: JPSS
ATTN: JPTM

DEPARTMENT OF DEFENSE (Continued)

National Security Agency
ATTN: B-43, C. Goedeke

Under Secy of Def for Rsch & Engrg
ATTN: Strat & Space Sys (OS)

DEPARTMENT OF THE ARMY

Army Logistics Management Ctr
ATTN: DLSIE

US Army Comm-Elec Engrg Instal Agency
ATTN: CC-CE-TP, W. Nair

US Army Communications R&D Command
ATTN: DRDCO-COM-RY, W. Kesselman

US Army Information Systems Cmd
ATTN: CC-OPS-W
ATTN: CC-OPS-WR, H. Wilson

US Army Material Command
ATTN: DRCLDC, J. Bender

DEPARTMENT OF THE NAVY

Naval Air Systems Command
ATTN: PMA 271

Naval Research Laboratory
ATTN: Code 4108, P. Rodriguez
ATTN: Code 4187
ATTN: Code 4700
ATTN: Code 4720, J. Davis
ATTN: Code 4780
ATTN: Code 6700
ATTN: Code 7500, B. Wald
ATTN: Code 7950, J. Goodman

Naval Telecommunications Command
ATTN: Code 341

Office of Naval Research
ATTN: Code 412, W. Condell

Space & Naval Warfare Systems Cmd
ATTN: Code 3101, T. Hughes
ATTN: Code 501A
ATTN: PDE-110-X1, B. Kruger
ATTN: PDE-110-11021, G. Brunhart
ATTN: PME 106-4, S. Kearney
ATTN: PME 117-20
ATTN: PME-106, F. Diederich

DEPARTMENT OF THE AIR FORCE

Air Force Geophysics Laboratory
ATTN: CA, A. Stair
ATTN: LIS, J. Buchau
ATTN: OPR-1

Air Force Weapons Laboratory
ATTN: NTN
ATTN: SUL

DEPARTMENT OF THE AIR FORCE (Continued)

Air University Library
ATTN: AUL-LSE

Ballistic Missile Office/DAA
ATTN: ENSN
ATTN: ENSN, W. Wilson
ATTN: SYC, D. Kwan

Deputy Chief of Staff, Rsch, Dev & Acq
ATTN: AF/RDQI
ATTN: AFRDS, Space Sys & C3 Dir

Electronic Systems Division
ATTN: SCS-1E
ATTN: SCS-2, G. Vinkels

Rome Air Development Center
ATTN: EEP, J. Rasmussen
ATTN: EEPS, P. Kossey

Strategic Air Command
ATTN: NRI/STINFO
ATTN: SAC/SIZ
ATTN: XPFC
ATTN: XPFS
ATTN: XPQ

DEPARTMENT OF ENERGY

University of California
Lawrence Livermore National Lab
ATTN: Technical Info Dept Library

OTHER GOVERNMENT AGENCY

Institute for Telecommunications Sciences
ATTN: A. Jean
ATTN: W. Utlaut

DEPARTMENT OF DEFENSE CONTRACTORS

Austin Research Associates, Co
ATTN: B. Moore
ATTN: J. Thompson
ATTN: J. Uglum
ATTN: M. Sloan

Autometric, Inc
ATTN: C. Lucas

Berkeley Research Associates, Inc
ATTN: J. Workman
ATTN: S. Brecht

University of California at San Diego
ATTN: H. Booker

DEPARTMENT OF DEFENSE CONTRACTORS (Continued)

EOS Technologies, Inc
ATTN: B. Gabbard
ATTN: W. Lelevier

Johns Hopkins University
ATTN: Dr. R. Greenwald

Kaman Tempo
ATTN: DASIAC
ATTN: B. Gambill

Kaman Tempo
ATTN: DASIAC

Maxim Technologies, Inc
ATTN: J. Marshall
ATTN: R. Morganstern

Mission Research Corp
ATTN: D. Knepp
ATTN: G. McCartor
ATTN: R. Bogush
ATTN: S. Gutsche
ATTN: Tech Library

Mitre Corp
ATTN: M. Horrocks

Pacific-Sierra Research Corp
ATTN: E. Field, Jr
ATTN: H. Brode, Chairman SAGE

Pacifica Technology
ATTN: E. Giller

Pennsylvania State University
ATTN: Ionospheric Research Lab

Physical Research, Inc
ATTN: J. Devore
ATTN: J. Thompson
ATTN: K. Schlueter

SRI International
ATTN: C. Rino
ATTN: D. Nielson
ATTN: G. Smith
ATTN: M. Baron
ATTN: R. Leadabrand
ATTN: R. Tsunoda
ATTN: W. Chesnut
ATTN: W. Jaye
2 cy ATTN: G. Price

Visidyne, Inc
ATTN: J. Carpenter

END
FILMED
4-86
DTIC